

Hilbert Curve-Based Metasurface to Enhance Sensitivity of Radio Frequency Coils for 7-T MRI

Smruti Ranjan Swain¹, Narendra Kumar Rout² and Madhushree Kuanr³

^{1,3}Associate Professor, Department of Computer Science Engineering, Gandhi Institute For Technology (GIFT), Bhubaneswar

²Assistant Professor, Department of Computer Science Engineering, Gandhi Engineering College, Bhubaneswar

Publishing Date: 4th March, 2018

Abstract— In this paper, we propose a compact, lightweight, and easy-to-fabricate Hilbert curve-based metasurface resonator that can effectively increase the sensitivity (radio frequency (RF) field intensity) and penetration depth of an RF coil for 7-T magnetic resonance imaging scanner. A circuit model is proposed to accurately calculate the resonance frequency of Hilbert curve resonators of different orders. A single element of a transverse electromagnetic (EM) coil was used for this paper. The increase in the field sensitivity introduced by the proposed metasurface to an RF coil was successfully demonstrated through simulations and experiments. The EM field produced by the RF coil is redistributed due to the presence of the proposed metasurface. The key feature of the proposed structure is its significant increase in the penetration depth of magnetic fields into the imaging volume. An enhancement of the magnetic field by more than four times was observed at 13.5 cm away from the coil experimentally. Flexibility for matching the coil integrated with the proposed surface is shown.

Index Terms— Hilbert curve, magnetic resonance imaging (MRI), metasurface, radio frequency (RF) coil.

I. INTRODUCTION

MAGNETIC resonance imaging (MRI) is a technique widely used for noninvasive diagnostic medicine, neuroscience, and biology [1]. In an MRI system, receive coils with high sensitivity (high B_1 field) guarantee strong signals for a quality image reconstruction [2]. The two commonly used types of receive coils are surface and volume coils. The first one can be placed close to the region of interest and strong signal can be obtained with low noise. However, the sensitivity of the coil degrades fast with the penetration depth and the signal from deeper tissue regions is hard to detect. The second type is used when a larger area/volume needs to be scanned. The signal from deeper regions of interest can be detected; however, as the dimensions of the coil increase, the signal-to-noise ratio (SNR) decreases due to the increased noise level. If the B_1 field of an RF coil could be manipulated and enhanced, it will increase the sensitivity and propagation depth of the coil, which would benefit the image quality of both surface and volume coils.

Manuscript received May 4, 2018; revised August 31, 2018; accepted October 29, 2018. This work was supported by the SUTD-ZJU/RES/04/2014 Research Grant. (Corresponding author: Elizaveta Motovilova.)

The authors are with the Engineering Product Development Pillar, Singapore University of Technology and Design, Singapore 487372 (e-mail: elizaveta@mymail.sutd.edu.sg; huangshaoying@sutd.edu.sg).

Color versions of one or more of the figures in this paper are available online at <http://ieeexplore.ieee.org>.

Digital Object Identifier 10.1109/TMTT.2018.2882486

Metamaterials and their 2-D counterparts, metasurfaces, are composite structures that can exhibit extraordinary properties not observed in natural materials. The elements of the metamaterials and metasurfaces are typically arranged in a periodic structure with the size of the resonant element smaller than the wavelength of the working frequency. Effective permittivity and permeability of metamaterials that are “seen” by the electromagnetic (EM) waves arise from their structure rather than just from the material properties. The engineering and applications of metamaterials and metasurfaces in microwave and RF frequency bands have been progressed rapidly in the past two decades [3]–[6]. These artificial composite materials show the unprecedented capability of manipulating EM waves when their design is strategically optimized for a particular application [7]–[9].

The ability of metamaterials to manipulate EM fields can especially be beneficial for MRI if the manipulation of the spatial distribution of RF field can be applied to increase the sensitivity of receive coils and to lower specific absorption rate (SAR) levels for MRI safety.

One of the first works to show the compatibility and potential usefulness of metamaterials for MRI was done by Wiltshire *et al.* [10]. In this paper, an array of swiss rolls was used as a magnetic flux guide to translate the signal from a sample to a distant receive coil which allowed imaging of a thumb with a distant surface coil [10]. In this approach, the SNR strongly depends on the geometry of the array and the coupling between the array and the receive coil. Moreover, the length of the array is 20 cm, which is bulky for the limited space in the bore of an MRI scanner. Later, a lens made of split rings was proposed in [11] to improve the coil sensitivity and its effectiveness. An enhancement of four times was reported in the region of 1–6 cm away from a loop coil. The key advantage of the split-ring lens [11] over the swiss roll array [10] is the 3-D isotropy and sensitivity to axial magnetic fields that allows manipulating the RF field in three directions.

In [12] and [13], a Fabry–Pérot resonator made of an array of parallel wires was proposed. The wire medium can transport evanescent waves, which carry subwavelength information, via their transformation into propagating waves inside the medium. This wire medium resonator can transport a transverse magnetic component of the RF field with practically no loss. Moreover, since the length of the structure should be a multiple of half a wavelength, collimation at very large distances can be obtained [13]. For the Fabry–Pérot resonator, the downside is that the total length of the wire medium

is 122 cm, which makes the structure impractical for the use in an MRI environment.

The physical size of metamaterials is the major limitation when they are applied to an RF system in an MRI scanner. The operating frequency of an intermediate (1–3 T) to ultrahigh-field (UHF >7 T) MRI scanner is in the range of approximately 40–400 MHz. Therefore, the size of a unit cell for metamaterials is in the centimeter to tens of centimeters range, which can often be impractical for the limited space available inside a scanner. To shorten the effective wavelength, and thus the unit cell size, high-permittivity materials, such as distilled water [14], [15] and CaTiO_3 [16], were used together with wire medium resonator demonstrating the improvement in the SNR and in the resolution of the MRI images. In [16], a field enhancement of two times was reported near the coil (<1 cm inside a load). Although high-permittivity materials lead to miniaturization of the metasurface, it requires special material preparation. Moreover, due to their physical properties, objects made of high-permittivity materials are usually heavy and bulky. It is challenging to design a compact and practical metamaterial/metasurface for MRI application.

In this paper, we propose a thin subwavelength ($< \lambda/10$) metasurface based on the Hilbert curve geometry for field enhancement of RF coils at 7 T. The proposed metasurface is planar so that it can be fabricated using the standard printed circuit board (PCB) technology.

In the literature, the Hilbert curve has already been proved to be helpful in the device miniaturization in the RF range, e.g., for antenna miniaturization at very high frequency (VHF) and ultrahigh frequency [17], for high impedance surface at gigahertz range [18], defected ground plane for filter designs [19], and RFID tags [20].

Due to the physical size limitations of the RF coils and the MRI bore, only one unit cell of Hilbert curve resonator is considered. Thus, more precisely, the proposed structure is a metasurface-like resonator. To facilitate the design and future application of the proposed approach, an accurate circuit model is proposed for a fast calculation of the resonance of a given Hilbert curve resonator.

The performance of the proposed structure in terms of the enhancement of coil sensitivity as a function of the order of the Hilbert curve and frequency is analyzed and compared based on realistic simulations. A single element of a transverse EM (TEM) coil and a fourth-order Hilbert curve unit cell were fabricated to operate at 297.2 MHz for 7-T MRI. A field enhancement of the RF coil is experimentally demonstrated.

The rest of this paper is organized in the following way. The Hilbert curve-based metasurface is introduced in terms of its circuit model and the resonance behavior in Section II. In Section III, the full-wave simulations of an RF coil with a Hilbert curve-based metasurface unit cell are presented and the field enhancement of the RF coil is shown. The experiment in terms of the setup and the results is detailed in Section IV. Discussion and conclusion are included in Sections V and VI, respectively.

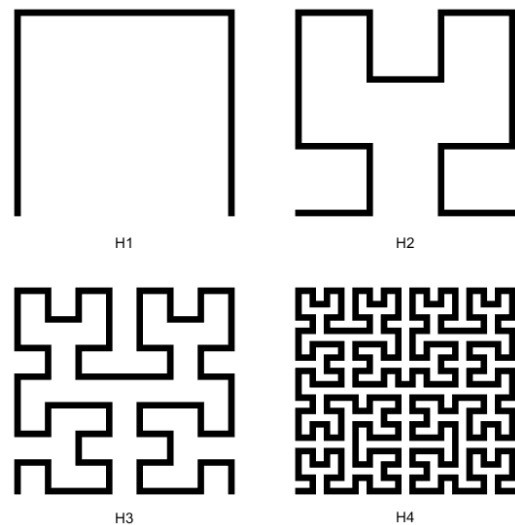


Fig. 1. Geometries of Hilbert curves of the first to the four orders, H_1 – H_4 .

II. HILBERT CURVE-BASED METASURFACE

Hilbert curve is one of the space-filling curves which is a mathematical concept used to describe a continuous planar curve constructed in such a way that it fills up a certain area, typically a square [21]. Fig. 1 shows the first four orders of a Hilbert curve, named H_n , where n is the order number ($n = 1, 2, 3, \dots$). It can be seen that as the order number increases, the structure becomes more complex and closely packed but remains nonself-intersecting. Applying Hilbert curve concept to RF designs, it means that a longer wavelength can be “folded” into the same area when the order number increases. Thus, higher order Hilbert curve structures can be applied for lower frequencies while maintaining a relatively small physical size. It is an important characteristic when it is applied as a resonator to enhance the field of an RF coil for MRI because the space inside an MRI bore is always limited and the compactness of the resonant structures is especially important.

A calculation of the resonant frequency is needed to design a Hilbert surface for an MRI RF coil. However, due to the growing complexity of its geometry with an increasing n , this becomes a challenging task. The resonant frequency of the Hilbert curve structure can be calculated using CST Microwave Studio Eigenmode solver (CST Studio Suit 2018), however, the 3-D numerical modeling and simulation can be time-consuming. In order to accelerate the calculation, we propose a circuit model that helps to quickly and accurately predict the resonance behavior of Hilbert curves of different orders.

A. Circuit Model

In the literature, a circuit model based on half-wavelength dipole was used to calculate the resonance frequency of a Hilbert curve resonator [17], [22]. Fig. 2 shows an illustration of the dipole model where all the U-turns are treated as short-circuited parallel wires (red dashed lines). The wires

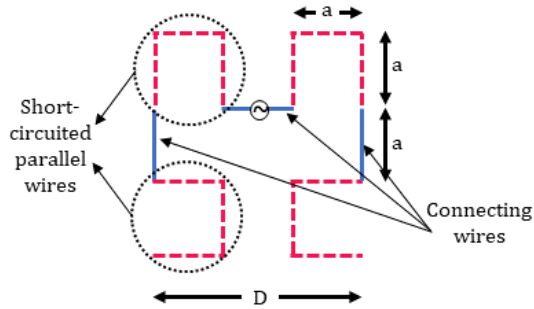


Fig. 2. Dipole-based circuit model for H_2 Hilbert curve unit cell using approach by Vinoy *et al.* [22].

connecting two successive U-turns are named the connecting wires (blue solid lines). In the dipole model, it is assumed that at the resonance, the input reactance of the given Hilbert curve equals that of a wire of length $\lambda/2$ [22]. In this model, it is also assumed that the input capacitance of the dipole antenna remains the same with the introduction of turns of the Hilbert curve resonator. This particular assumption will be further discussed in the next paragraph. Thus, the resonance condition for a dipole is expressed as follows [22]:

$$k \frac{\eta}{\pi \omega} \log \frac{2a}{d} \tan(\beta a) + \frac{\mu_0 b}{\pi} \log \frac{8b}{d} - 1 = \frac{\mu_0 \lambda}{\pi} \log \frac{2\lambda}{d} - 1 \quad (1)$$

where the left-hand side is the input inductance of the Hilbert curve resonator which is a sum of the inductance due to the U-turns and the self-inductance of the connecting wires. The right-hand side of (1) is the inductance of a half-wavelength wire. In (1), $k = 4^{n-1}$ is the number of short-circuited parallel wire sections, n is the order number of a Hilbert curve, η is the intrinsic impedance of free space, ω is the frequency of interest, β is the phase constant, a is the length of the wire sections as shown in Fig. 2, d is the diameter of wires, and $b = a(2^{2n-1} - 1)$ is the total length of all the connecting wires.

Fig. 3 shows the resonance frequencies of the Hilbert curve of different orders versus the length of a wire section, a . We have only considered the values of the parameter a up to 50 mm, as for larger values of a , the metasurface size becomes impractical for MRI application. The calculation was done using both CST Eigenmode solver (solid lines) and (1) [22]. The wire diameter is fixed to be $d = 2$ mm throughout all the calculations and simulations. In Fig. 3, it can be seen that the trends of the curves calculated using CST and that calculated using (1) agree with each other. However, a considerable discrepancy in the resonant frequency at each a is noted. Moreover, the difference becomes larger when a decreases which corresponds to a Hilbert curve of a greater compactness. Table I summarizes the relative error between the CST simulations and the calculations using (1). It is noted that using (1) fails to find the resonance frequency for the values of a below 7 mm.

This discrepancy could be caused by the unaccounted capacitive and inductive interactions between the neighboring wire segments. When the order goes higher and the geometry of

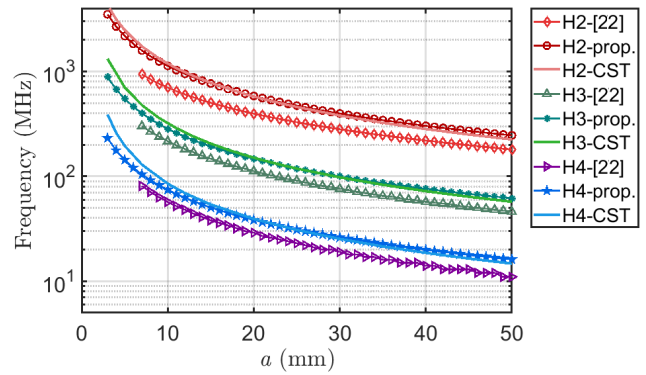


Fig. 3. Comparing CST eigenmode simulations and the circuit model calculations using [22] and the proposed optimized circuit model.

a Hilbert curve becomes more compact, as shown in Fig. 1, both the capacitive and inductive coupling of the neighboring wire segments increase considerably. The increase in mutual capacitance and mutual inductance needs to be taken into account in the calculation to increase the accuracy of the circuit model. Therefore, a better circuit model that takes care of the mutual interactions is needed, especially when the order of the Hilbert curve is high, and the wires segments are closely packed.

A new circuit model is proposed with improved accuracy. It is based on an equivalent dipole with both the input capacitance (C_t) and inductance (L_t) taken into consideration. At the resonance, the total reactance equals zero as follows:

$$X = j\omega L_t + \frac{1}{j\omega C_t} = 0. \quad (2)$$

Therefore, the resonant frequency can be obtained as

$$\omega_{\text{res}} = 1/\sqrt{L_t C_t}. \quad (3)$$

The total inductance includes self-inductance of all the wires and mutual inductance of parallel wires. There are two types of parallel wires. Using a third-order Hilbert curve as shown in Fig. 4 for an illustration, type 1 is the short-circuited parallel wires (shown in the inset on the left in Fig. 4) and type 2 is the parallel wires without a shorting wire (shown in the inset on the right in Fig. 4). They are both separated by a distance of a ; however, in [22], only type 1 was considered. Thus, for the proposed circuit model, the total inductance of the Hilbert curve resonator can be written as follows:

$$L_t = s_n L_s - 2m_n L_m \quad (4)$$

where L_s is the self-inductance of a wire of length a and s_n is the number of all the wire segments of the curve (each of length a), L_m is the mutual inductance of two wires with a distance of a , and m_n is the number of all the parallel wires (both types 1 and 2). Both s_n and m_n are determined by the order number n .

The total number of straight wire segments s_n can be found using the following progression for $n \geq 2$:

$$s_n = s_1 + 4s_{n-1} \quad (5)$$

TABLE I
RELATIVE ERROR (%)

		3	5	7	15	30	40	50
Vinoy et al. [22]	H2			45.8	35.5	26	22.4	19.8
	H3			37	28.3	22.2	21	19.5
	H4			37.3	29.4	24.9	24.8	25.2
This work (11)	H2	18.8	12.3	8.6	1.4	4.7	7.3	9.4
	H3	33.2	22.4	16.6	5.9	2.2	5.4	8
	H4	40.5	26.6	19.3	6.3	3.2	6.9	9.8

where $s_1 = 3$. The total number of parallel wire segments m_n is a sum of the number of the type 1 parallel wires $m_n = 4^{n-1}$ and that of type 2 wires, m , $m_n = m_n + m$. Number m does not have an analytic expression linking to n and has to be counted separately for each order number. Table II lists the numbers of different wire segments of a Hilbert curve for the first four orders.

The self-inductance of a round wire of length a and diameter d is given as [23]

$$L_s = 2 a \log \frac{a + \sqrt{a^2 + d^2/4}}{d/2} - \frac{a}{a^2 + d^2/4} + \frac{a}{4} + d/2 \tag{6}$$

where a and d are in centimeters (cm) and the inductance is in nanohenries (nH).

The mutual inductance of two parallel wires of length and separation p is given as [23]

$$L_m = 2 \log \frac{\sqrt{2 + p^2}}{2} - \frac{p}{2} + p \tag{7}$$

which in our case, $p = a$, and (7) can be simplified as follows:

$$L_m = 2[a \log(1 + \frac{\sqrt{2}}{2}) - a \frac{\sqrt{2}}{2} + a]. \tag{8}$$

The mutual capacitance of two parallel wires is given as [24]

$$C_m = \frac{\pi a}{\text{arcosh}(a/d)} \tag{9}$$

where the length is expressed in meters (m) and the capacitance in farads (F). The total capacitance can then be calculated as $C_t = m_n C_m$.

The resulting equation for the resonance frequency of the Hilbert curve of order n is the following:

$$\omega_{\text{res}} = 1/\sqrt{m_n C_m (s_n L_s - 2m_n L_m)}. \tag{10}$$

Equation (10) was used to calculate the resonant frequency of H_2 , H_3 , and H_4 curves with the same parameters as those in the previous calculations. It is noticed that the proposed formulation can better approximate the resonance behavior of H_2 curve. However, there is a significant discrepancy for higher orders. This can be caused by the increased compactness of the structure when the order number is increasing. In (10), only the parallel wires that are immediate neighbors are accounted for. However, when the order number increases while the area the curve covers stays the same, the geometry of

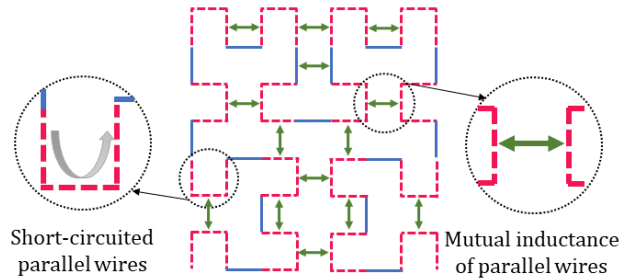


Fig. 4. H_3 Hilbert curve unit cell.

TABLE II
NUMBERS OF WIRE SEGMENTS IN A HILBERT CURVE

n	m	m	m
1	3	1	0
2	15	4	2
3	63	16	14
4	255	64	69

the curve becomes more compact and the interaction between the nonimmediate neighbors starts to play a role.

The effect of the increasing compactness and interaction between the segments can be accounted for with a modification on the parameter m_n in the following way, $m_n^* = m_n + \log(n \cdot m_n)$. The resulting resonance formula now becomes

$$\omega_{\text{res}} = 1/\sqrt{m_n^* \cdot C_m s_n L_s - m_n^* \cdot L_m}. \tag{11}$$

The resonant frequency versus the segment length a for H_2 , H_3 , and H_4 Hilbert curve resonators using the modified proposed circuit model, expressed as (11), is compared to the simulated results in Fig. 3 and Table I. As can be seen in Fig. 3 and Table I, the calculation using the modified proposed method agrees well with the eigenmode results for Hilbert curves of different orders. Moreover, unlike the model in (1), which fails to find the resonance frequency of a Hilbert curve when $a < 7$ mm, the proposed method (11) provides calculation accuracy for all values of parameter a . When a is very small, it is observed that the discrepancies between the proposed method and that obtained from the CST simulation increase considerably (up to 40.5% in the H_4 case). More complex weighting functions are needed when a goes below 5 mm. The average relative error between the eigenmode simulated results and results calculated using (11) is 7.6%, 11.5% and 14.2%, compared to the error of 31.7%, 26.1%, and 28.7% when using (1) for the H_2 , H_3 , and H_4 curves, respectively. The specific relative error for a given a is summarized in Table I.

The calculation speed of the proposed model (11) is evaluated using MATLAB R2018a on a standard desktop computer (Intel Core i7 processor with 32-GB RAM). It should be noted that the time required to calculate one resonance mode in CST depends greatly on the order number n and the dimensions of the curve. For example, to calculate the resonance of a Hilbert curve of area 50 mm × 50 mm, CST needs

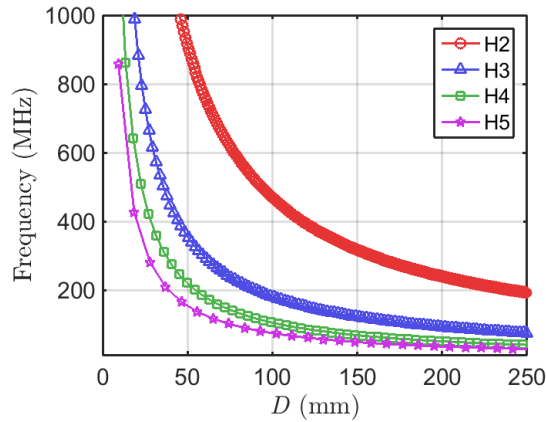


Fig. 5. Resonance frequency versus the total size D of Hilbert curve unit cell of different orders.

54, 147, and 359 s for the H_2 , H_3 , and H_4 curves, respectively. For the same structures of a larger area of $100 \text{ mm} \times 100 \text{ mm}$, CST needs 85, 243, and 807 s for the H_2 , H_3 , and H_4 curves, respectively. On the other hand, the proposed method (11) allows to calculate the whole resonance curve for a given wire diameter within several milliseconds. The calculation speed is much higher by using the proposed model compared to that using CST.

B. Resonance Behavior

Using the proposed circuit model, the resonance behavior of the Hilbert curve resonator can be studied within a practical time. The resonance frequencies versus the total length of a unit cell, D (as shown in Fig. 2), of Hilbert curves of different orders were calculated and plotted in Fig. 5. The diameter of the wire was kept the same throughout the calculations ($d = 0.1 \text{ mm}$). In Fig. 5, it can be seen that with an increase in the order n , the curves move closer to the two axes. This indicates that it is possible to make a more compact resonator at lower frequencies by using a Hilbert curve of higher order. It is also observed that the movement of the curve decreases rapidly when the order increases, so does the size reduction at a fixed frequency. Taking 300 MHz as an example, the total size of a unit cell decreases from 160 mm ($0.16\lambda_0$) to 59 ($0.059\lambda_0$), 37 ($0.037\lambda_0$), and 26 mm ($0.026\lambda_0$) from H_2 to H_3 , H_4 , and H_5 , respectively. When the order increases, the electrical length of a Hilbert curve cell reduces from more than $1/10\lambda$ to about $1/40\lambda$. On the one hand, the electrical length decreases dramatically when the order goes higher. On the other hand, it implies that the size reduction is saturating at higher orders. Thus, further increasing the order after H_5 may not provide a significant reduction of the cell size. Instead, it will increase the complexity of the curve. Moreover, with high compactness, the width of the wire needs to be reduced to mitigate the cancellation of fields of the wire sections at close proximity to maintain the resonance of the structure. This will be further discussed in Section V.

C. Hilbert Curve as a Metamaterial

A metamaterial with a negative refraction index discovered by Pendry [8] is able to focus EM field and provide

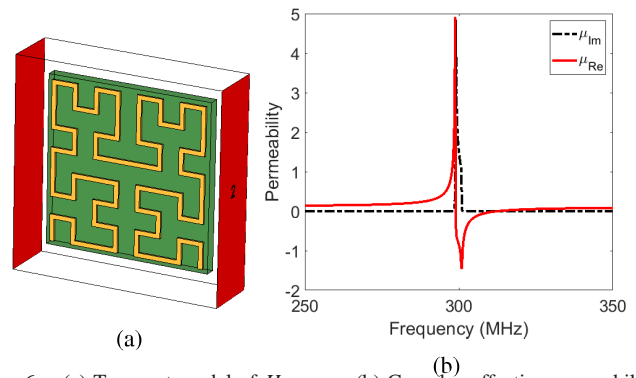


Fig. 6. (a) Two-port model of H_3 curve. (b) Complex effective permeability of H_3 curve with $a = 11 \text{ mm}$.

subwavelength resolution. To observe this effect in a near-field application, such as MRI, only one of the material properties (ϵ or μ) needs to be negative [25]. To demonstrate the negative permeability of a Hilbert curve, a two-port system with H_3 curve as an example was modeled in CST Microwave Studio as shown in Fig. 6(a). The H_3 curve is modeled as perfect electric conductor (PEC) on an FR4 substrate ($\epsilon_r = 4.3$, $\tan\delta = 0.025$) located between two waveguide ports. Orthogonal electric and magnetic boundary conditions are applied. Based on Fig. 3, the parameter a was chosen to be 11 mm such that the H_3 curve resonates at 300 MHz. Fig. 6(b) shows the extracted real and imaginary parts of the effective permeability based on the calculated S-parameters [26]. In Fig. 6(b), negative permeability is observed at the resonance at 300 MHz. It demonstrates the metamaterial behavior of a Hilbert curve resonator.

III. FULL-WAVE SIMULATIONS

The proposed Hilbert curve-based unit cell metasurface resonator is applied to an MRI RF coil to enhance its field strength. 7-T scanner with operating frequency of 297.2 MHz was chosen to demonstrate the effectiveness of the proposed metasurface. Application of the Hilbert curve resonator can be considered for other lower field scanners as well, such as 1.5 and 3 T. In order to study the effectiveness of field enhancement due to the proposed metasurface to an RF coil, full-wave simulations using CST Microwave Studio were performed. The metasurface is placed between the target under a scan and the coil. The dimension of the metasurface is approximated based on the proposed circuit model and later fine-tuned to account for the coupling from the coil that is in proximity to the unit cell metasurface.

A. 3-D Model

A 3-D model shown in Fig. 7 is constructed for the study. Fig. 7(a) and (b) shows the 3-D view and the side view of the model. It consists of a microstrip line (MTL) that is one of the independent elements constituting a TEM coil [27] (it is named MTL coil in this content), a metasurface, and a load. The MTL coil was chosen for this investigation because the TEM coil is a widely used and studied volume coil for the UHF MRI [2].

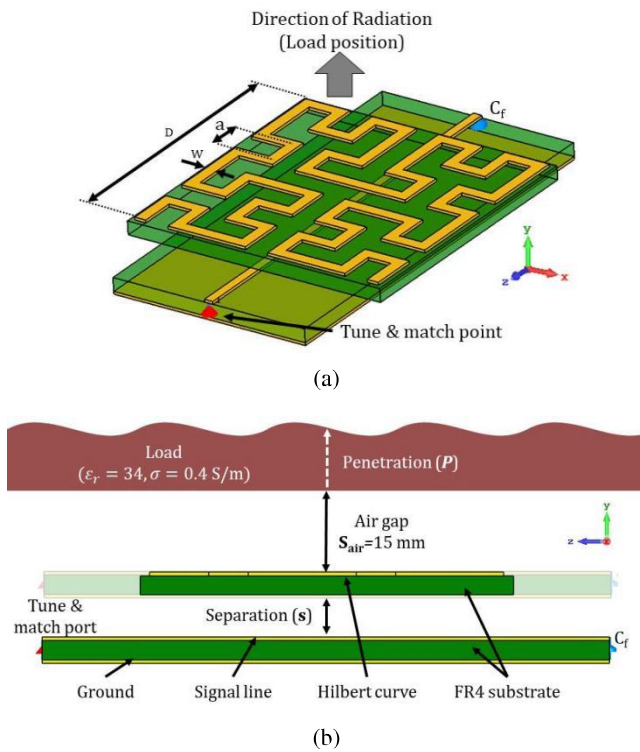


Fig. 7. MTL coil with the proposed metasurface. (a) 3-D view. (b) Side view.

However, other single-channel coils could be considered as well, such as loop or dipole coils. The dimensions of the MTL coil are chosen for the application for human head imaging. PEC is used for the ground plane ($7.5 \text{ cm} \times 15 \text{ cm}$) and the signal line ($0.3 \text{ cm} \times 15 \text{ cm}$), and a standard FR4 ($\epsilon_r = 4.3, \tan\delta = 0.025$) substrate ($7.5 \text{ cm} \times 15 \text{ cm} \times 0.16 \text{ cm}$) is chosen for the model. The MTL coil is loaded with a capacitor C_f and tuned and matched using a shunt C_t and series C_m variable capacitors. The coil is tuned and matched to resonate at 297.2 MHz for a 7-T scanner.

The specific values of capacitance vary in the range from 1 to 35 pF depending on the geometry of the metasurface under consideration. The metasurface is comprised of one unit cell of the Hilbert curve, and different orders are considered for simulations. The Hilbert curve was set to be PEC on an FR4 substrate and placed above the MTL coil. The distance between the metasurface and the signal line of the MTL coil is denoted as s . The load is a homogeneous cuboid ($40 \text{ cm} \times 40 \text{ cm} \times 20 \text{ cm}$) with electrical properties of $\epsilon_r = 34$ and $\sigma = 0.4 \text{ S/m}$ that represent the average tissue properties of human body [28]. As safety regulations for the MRI RF coils require an isolation between a coil and a subject under a scan, an air gap between the metasurface and the bottom of the load S_{air} is introduced and is kept equal to 15 mm throughout all the simulations. The penetration depth from the bottom of the cuboid into the load is denoted as P . In the case of the MTL coil without a metasurface, the coil is shifted closer to the load and replacing the metasurface as shown with a transparent drawing in Fig. 7(b). This is done to fairly compare the performance of the system with and without the

proposed metasurface. This model is used for all full-wave EM simulations unless otherwise specified.

After obtaining the resonant frequency of the Hilbert curve-based unit cell resonator of different orders from the circuit model, as shown in Fig. 5, the dimension of a unit cell is chosen to be smaller or equal to an RF coil working at 297.2 MHz for field enhancement. Due to the coupling from the coil, the resonant frequency of the unit cell metasurface and the coil is shifted when they are placed close to each other. With a fixed relative location with the coil, the unit cell metasurface is fine-tuned to resonate at the targeted frequency. The sizes of the resonating unit cells of H_2 – H_4 Hilbert curves are $12.24 \times 12.24 \text{ cm}^2$, $11.40 \times 11.40 \text{ cm}^2$, and $10.92 \times 10.92 \text{ cm}^2$. They all have a comparable physical size with the MTL coil. After a comparative analysis, the H_4 curve resonator was chosen for further investigations as it can provide the most compact solution.

B. Simulation Results

The scattering parameter S_{11} of the MTL coil and the 3-D EM field distributions in the modeling domain were calculated when an H_4 Hilbert curve unit cell was introduced in close proximity to the coil. An optimization of the Hilbert curve dimensions (a and w) was performed in order to find the best compromise between maximizing the average B_1^+ -field over the load volume and minimizing the maximum SAR (1 g averaged). The optimal dimensions were found to be $D = 10.92 \text{ cm}$, $a = 7 \text{ mm}$, and $w = 5 \text{ mm}$.

The simulated 2-D B_1^+ -field distributions for the MTL coil with and without the H_4 metasurface are shown in Fig. 8, where the first, second, and third rows show the field distributions on the xy plane ($z = 0 \text{ mm}$), the yz plane ($x = 0 \text{ mm}$), and the xz plane ($P = 100 \text{ mm}$ inside the load), respectively. Note that the first colorbar is valid for the xy and yz planes, while the second colorbar applies only to the xz plane. Comparing the field distributions of the first two rows, it can be seen that with the H_4 metasurface added, the field penetrates deeper into the load. This can easier be seen from the field distributions of a plane deep into the load, as those shown in the third row in Fig. 8. As can be seen in Fig. 8(e) and (f), on a plane 100 mm into the load, the B_1^+ -field is redistributed and becomes stronger with the introduction of the H_4 metasurface resonator.

Fig. 9 shows the simulated SAR distributions. The first row shows the SAR distributions on the xy plane when $z = 0 \text{ mm}$. It can be seen that with the introduction of H_4 metasurface resonator, the SAR is redistributed such that the peak value significantly decreases and the peak SAR region is split from one peak at the center to two symmetrical peaks. The locations of the peak values were found to be at $x = 0 \text{ mm}$ for the MTL coil without metasurface and $x = 40 \text{ mm}$ for the MTL coil with a metasurface both of which are indicated by a white dashed line. Fig. 9(c) and (d) shows the SAR distributions on the yz plane that goes through the corresponding peak SAR lines in Fig. 9(a) and (b), respectively. The total maximum SAR (1 g averaged) was found to be 1.39 W/kg for the MTL coil alone and it is reduced to 0.48 W/kg for the MTL coil

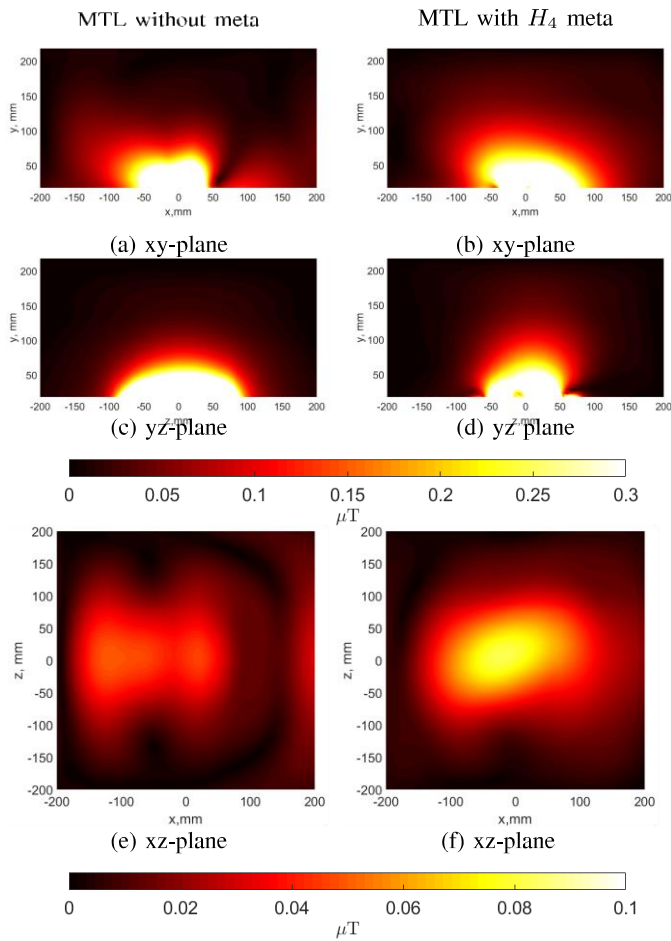


Fig. 8. Simulated B_1^+ -field distribution on the xy , yz , and xz planes, in μT , normalized to 1 W of delivered power. (a), (c), and (e) MTL coil without metasurface. (b), (d), and (f). MTL coil with H_4 metasurface.

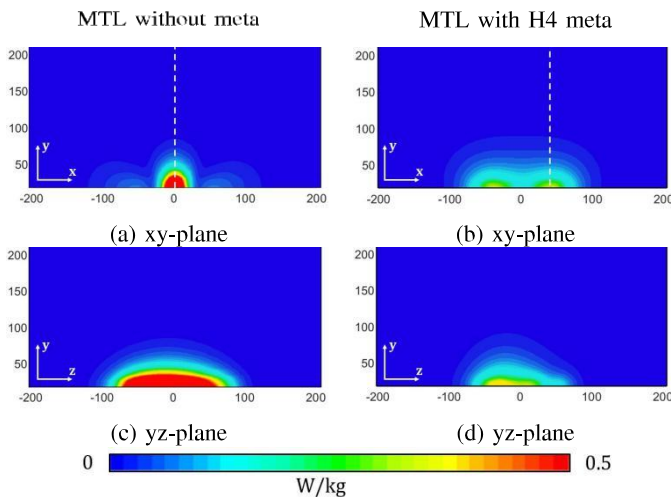


Fig. 9. Simulated SAR distribution on the xy and yz planes. (a) and (c) MTL coil without metasurface. (b) and (d) MTL coil with H_4 metasurface.

with H_4 metasurface resonator, which means a 66% decrease in the maximum SAR level with the introduction of the Hilbert curve resonator.

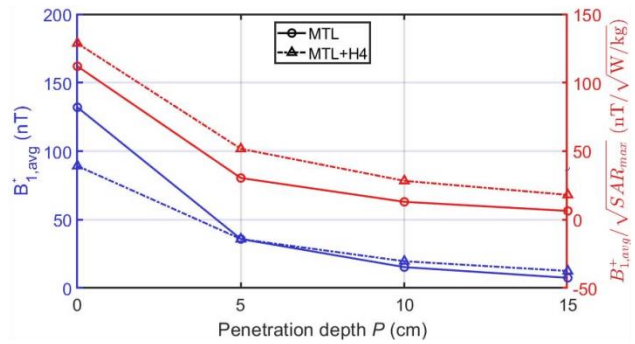


Fig. 10. Left-hand side axis (blue lines): $B_{1,avg}^+$ field versus penetration depth P with and without H_4 metasurface at 7 T. Right-hand side axis (red lines): $B_{1,avg}^+ / \sqrt{SAR_{max}}$ field versus penetration depth P with and without H_4 metasurface at 7 T.

Next, the average B_1^+ -fields at four xz planes inside the load: $P = 0$ cm, $P = 5$ cm, $P = 10$ cm, and $P = 15$ cm, are examined. All the field values were further normalized to the corresponding maximum SAR levels (1 g averaged).

Fig. 10 shows the average $B_{1,avg}^+$ -field versus P on the left and $B_{1,avg}^+ / \sqrt{SAR_{max}}$ [the same $B_{1,avg}^+$ -field normalized to the square root of the corresponding maximum SAR levels (1 g averaged)] on the right, with and without H_4 metasurface.

For $B_{1,avg}^+$, it can be seen that even though the field intensity decreases for both cases when the wave propagates into the load, the decay rate is slower for the MTL with the H_4 metasurface and the wave penetrates deeper into the phantom. For $B_{1,avg}^+ / \sqrt{SAR_{max}}$, when SAR is taken into consideration, it can be seen that with the introduction of the H_4 unit cell metasurface, the MTL coil shows significant increase in the maximum SAR-normalized $B_{1,avg}^+$ compared to the MTL coil without a metasurface. In particular, the field strength is improved by 15%, 66%, 118%, and 184% at the distance of 0, 5, 10, and 15 cm into the phantom, respectively.

To further illustrate the improvement in RF field sensitivity, the distribution of $B_1^+ / \sqrt{SAR_{max}}$ on an xz plane at the penetration depth $P = 10$ cm inside the load is plotted and shown in Fig. 11. As can be observed, due to a lower maximum SAR level, the MTL coil with H_4 metasurface produces a stronger and more spread-out B_1^+ distribution.

The separation between the metasurface and the coil affects the reflection at the input of an RF coil. This provides a degree of flexibility to tune the MTL coil. Fig. 12 shows the shift in the resonance frequency with respect to the separation between the MTL coil and the H_4 metasurface resonator. The black dashed line shows the S_{11} -parameters when the MTL coil is tuned and matched to 297.2 MHz without any metasurface. When the H_4 metasurface resonator is placed directly on the MTL coil ($s = 0$, the curve with round markers), the resonance is shifted approximately 24 MHz toward the lower frequencies. This is due to the mutual inductance introduced between the metasurface and the coil when the latter is placed on the top of the coil. This can be explained by considering the resonance formula $\omega = 1 / \sqrt{LC}$. When the metasurface is placed close to the coil (dark blue circle line), the introduced mutual inductance between the two elements is the largest,

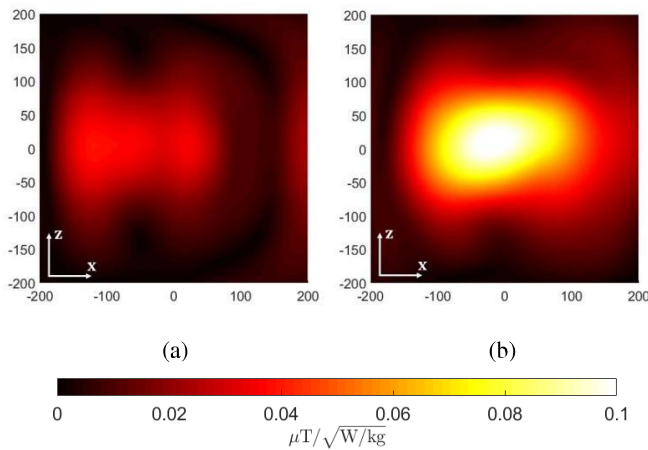


Fig. 11. Simulated $B_{1,avg}^+ / (\text{SAR}_{\text{max}})^{1/2}$ at penetration depth $P = 10$ cm inside the load for MTL coil (a) without metasurface and (b) with metasurface H_4 .

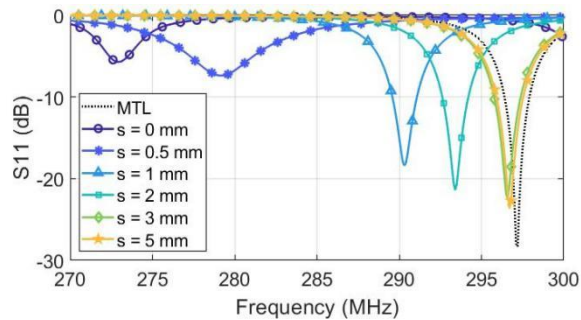


Fig. 12. S_{11} parameter drift with respect to the separation distance s .

thus it shifts the resonance to the lowest frequency. When the separation between the two elements is increased (lighter blue color lines), the mutual inductance decreases, and the resonance frequency increases. By changing s , the RF coil can be tuned to match at the desired working frequency.

IV. NEAR-FIELD MEASUREMENTS

In order to validate the simulation results, H - and E -field distributions were measured in free space with and without the metasurface. The corresponding model was created in CST without a load to compare with the measurements (same as in Fig. 7 but without the load).

A. Near-Field Measurement Platform

Fig. 13 illustrates the experimental setup, where the magnetic field distribution is measured indirectly by measuring S_{21} parameter of the structure under test (SUT), which consists of the MTL coil and the metasurface placed directly above it. The SUT is driven through Port 1 of the vector network analyzer (VNA, Rhode & Schwarz ZVH8). The field probe is connected to Port 2 of the VNA. For the magnetic field measurements, two loop probes from Langer EMV-Technik RF 2 set were used. The smallest probe RF-B 3-2 of the aperture approximately 4 mm was used to capture the normal component of the magnetic field H_y . The other probe RF-R 50-1 of aperture

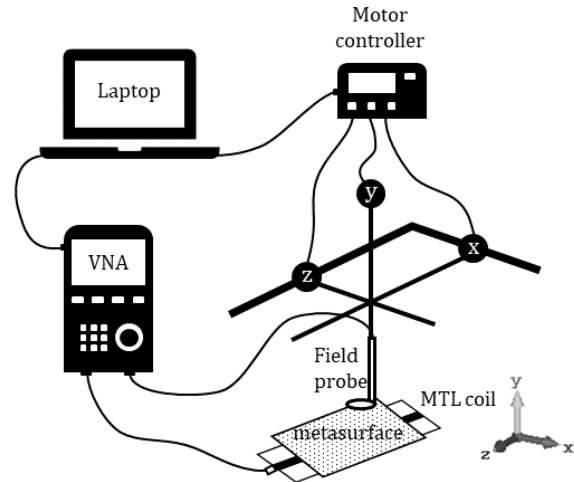


Fig. 13. Measurement setup.

10 mm was used to capture the perpendicular component of the magnetic field H_x . Even though other field components can be measured as well by rotating the loop probe to be normal to the corresponding field orientation, the mentioned field component's distributions can substantially provide a validation.

The electric field can be measured in a similar manner with an open coaxial probe. The coaxial probe is, in principle, a capacitive probe. The electric current induced in the probe is mainly due to the normal component of the E -field [29]. Thus, only E_y -field component can be measured.

When choosing the aperture of the probe, a tradeoff between the resolution and the noise has to be considered. When the size of the probe is relatively small, such as the RF-B 3-2 probe, the resolution can be comparable to an ideal simulated case; however, the effects of the background noise can be significant. On the other hand, the larger probe gives better contrast, however, the resolution suffers [30].

An in-house built measurement platform with three-axis movements (x -, y -, and z -axes) was used. It allows the probe to move in a maximum region of $50 \text{ cm} \times 50 \text{ cm} \times 50 \text{ cm}$. The S_{21} -parameters were measured at the xz plane that is 15 mm above the metasurface with the step size fixed at 2 mm. The cables connected to the VNA are 1 m long to ensure a smooth, unconstrained movement of the probe. Cylindrical ferrite cores were attached to the cables in order to avoid any parasitic signals and unwanted noise.

The free-space measurements were compared with the simulations of the coil with and without metasurface in the absence of the load (in air). It should be noted that even though the free-space measurements do not represent the real operating environment of MRI, these measurements are still useful as they validate the accuracy of the modeling and validate the enhancement of the RF fields introduced by the proposed metasurface to an MRI RF coil.

B. Prototype Fabrication

For the experiment, the proposed Hilbert curve-based metasurfaces and an MTL coil were fabricated.

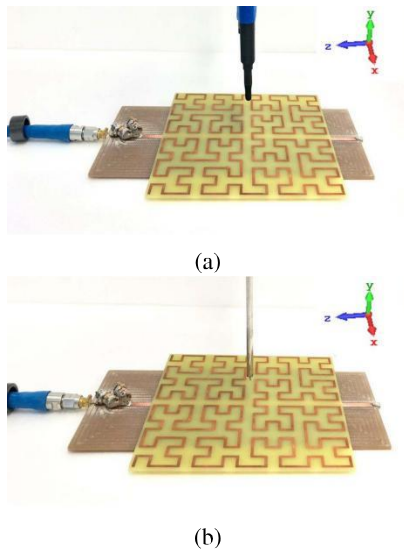


Fig. 14. Fabricated prototype of H_4 metasurface on MTL coil with (a) H -field probe and (b) E -field probe.

FR4 PCB ($\epsilon_r = 4.3, \tan\delta = 0.025$, substrate height $h = 1.554$ mm, and copper thickness $th = 0.035$ mm) was used. Fig. 14 shows a photograph of the fabricated MTL coil and an H_4 metasurface resonator. The metasurface is positioned directly on the top of the MTL coil. The MTL coil was connected to Port 1 of the VNA through a tuning and matching network and loaded with a fixed value capacitor of 5 pF (Dalicap). Two 5.5–20-pF trimmers (Sprague-Goodman) were used to fine tune the coil to 50 MHz. The H -field probe was connected to Port 2 of the VNA. As the measurements were done outside the actual scanner environment, a ferrite instead of a balun was used to prevent the common mode currents on the cable shield.

C. Measurement Results

Fig. 15 shows a comparison of the measured and simulated distributions of E_y and H_y . All of the fields are normalized to display the maximum value of 1 on a linear scale. The measurement plane is 15 mm away from the metasurface. The step size was set to be 2 mm for the E_y -field and the H_y -field. The simulated E_y and H_y were exported from CST with the same resolution of 2 mm for a fair comparison. Comparing the left column to the right column in Fig. 15, the simulated electric/magnetic field patterns agree well with the measured ones. The bright spot in the bottom of the measured H_y -field is due to the presence of the capacitors which cannot be accounted for in the simulations.

Fig. 16(a) and (b) shows the measured H_x -field distribution on the yz plane without and with the proposed metasurface, respectively. The resolution of the measurement was set to be 5 mm and the field values are displayed in arbitrary units (a.u.). Shading interpolation was used when plotting the field distribution. The vertical axis is the distance away from the coil. Comparing Fig. 16(a) to (b), it can be seen that the H_x -field is redistributed with the presence of the metasurface resonator. The field intensity close to the coil is weaker in

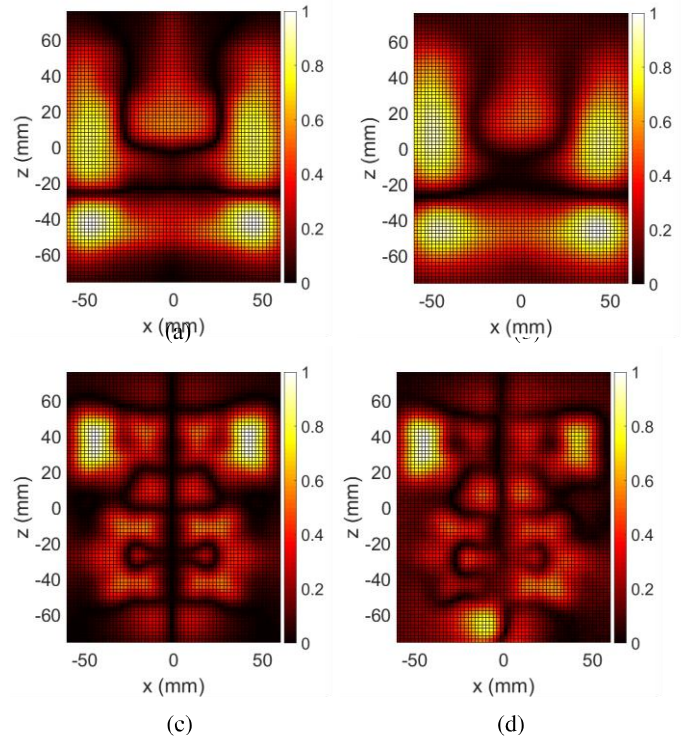


Fig. 15. Comparison of measured and simulated normal field components E_y and H_y on the xz plane. All the plots are normalized to display the maximum value of 1 on a linear scale. (a) E_y simulated. (b) E_y measured. (c) H_y simulated. (d) H_y measured.

the case of the coil coupled with the metasurface. However, the field propagates further away from the coil with the metasurface in place and its intensity decays at a slower rate. For example, at the penetration depth of 65 mm, the average H_x -field is 1.2 and 1.6 a.u. in the case of the MTL alone and the MTL with metasurface, respectively, which means a 33% improvement in intensity. At the further depth of 135 mm, the average H_x -field is 0.13 and 0.57 a.u. in the case with and without a metasurface, respectively. This corresponds to an improvement of more than four times. The penetration of waves is significantly enhanced by the proposed structure. In a *in vivo* setup, when the same amount of loss is added to the penetration path, it may outperform the reported structures in the literature where an enhancement of four times was reported at a distance of 6 cm from the coil in [11] and in the distance of less than 1 cm in [16]. The SNR of the H_x -field on the xz plane was calculated using the following formula:

$$\text{SNR} = 10 \cdot \log_{10}[\text{mean}(\text{signal})/\text{STD}(\text{noise})]. \quad (12)$$

Based on (12), $\text{SNR}_{\text{MTL}} = 15.75$ and $\text{SNR}_{\text{meta}} = 17.24$ in the case of MTL coil alone and MTL coil with the proposed metasurface, respectively. Fig. 16(c) compares the field propagation away from the coil at several locations of z . It can be observed that at the distances above 5 cm away from the coil, the MTL coil paired with the proposed metasurface outperforms the single MTL coil in all the cases. The average

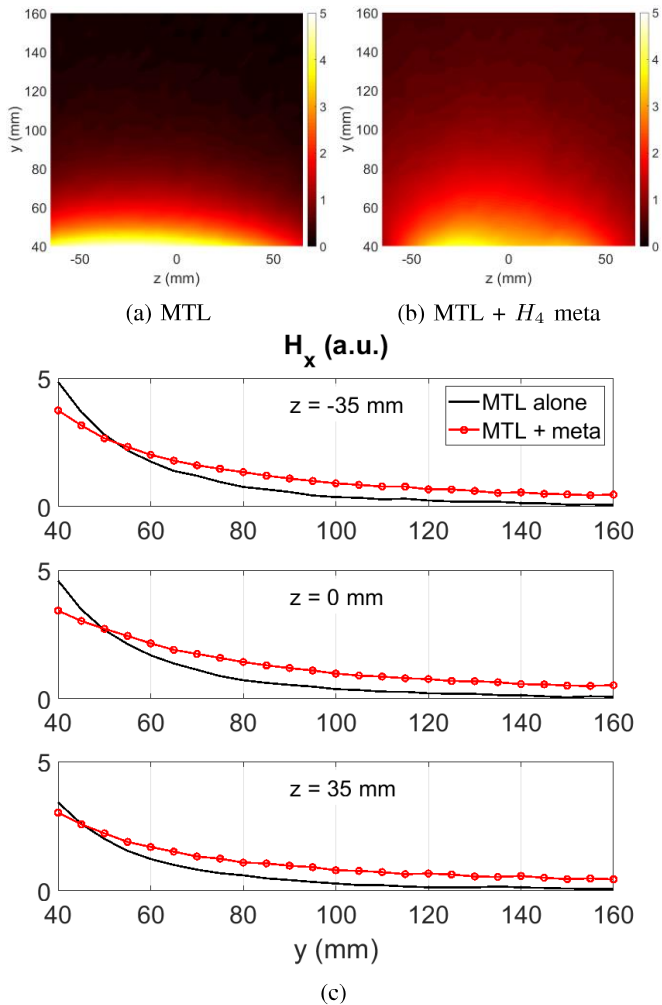


Fig. 16. Comparison of measured H_x -field distributions in air (a) without and (b) with the H_4 metasurface resonator. (c) Measured H_x -field along the y -direction at several z positions.

improvement is 20%, 32%, and 42% at $z = -35$ mm, $z = 0$ mm, and $z = 35$ mm, respectively.

V. DISCUSSION

The proposed metasurface has the advantages of providing a long penetration into the imaging volume, being planar and compact, easy to fabricate using the standard PCB technology. Strictly speaking, the metasurface presented in this paper is not a true metasurface as it consists of only one unit cell. However, it has been shown that it resonates and effectively enhances the RF field of an RF coil (the coil sensitivity). It is a first step in the discovering of the properties of such a system: a standard coil coupled with a resonator based on the Hilbert curve that together can beneficially alter the RF field for an enhancement. As the wavelength of the corresponding working frequency is comparable to the dimensions of an RF coil in an MRI system, a larger number of unit cells may be impractical. However, it is still important to investigate the behavior of such a system when the resonator has one or more than one unit cell and it (they) resonates and enhances the field strength of an RF coil.

A potential improvement could be the use of a double-sided configuration, where the Hilbert curve is printed on both sides of the substrate. The relative orientation of the Hilbert curves on different sides can be changed to manipulate the field distributions [31].

Introduction of a via could lead to a longer effective electrical length and thus can help with the miniaturization of a unit cell.

The variation of distance changes the reflection coefficient at the input of the coil (as shown in Fig. 12). This offers a degree of freedom for coil tuning and matching when a metasurface is introduced to an existing MRI coil.

It should be noted that even though Fig. 5 shows the potential to reduce the size of a Hilbert curve-based resonator by increasing the order, the effectiveness of this configuration for the field enhancement drops if the width of the wire stays the same. The reason being that for higher order numbers, the straight wire sections become very closely spaced. This leads to the fact that the opposing currents at the close neighboring wire segments cancel each other out [32] and thus decrease the effective length of the wire. These factor starts to play a bigger role at higher Hilbert curve orders n and thus prevent the structure from resonating effectively. A remedy to this is to reduce the width of the wire.

In this paper, we only considered the application of the Hilbert curve-based metasurface resonator to a single MTL coil element, aiming to show the effectiveness of the field enhancement by introducing the proposed metasurface to the coil. This idea can be extended to other MRI coils such as loops [31], dipoles, and coil arrays. The effectiveness of the proposed metasurface to different coils and coil arrays needs to be further tested. The compatibility of the proposed structure to an MRI system needs to be addressed in detail in the near future. Phantom and *in vivo* studies are needed to validate the usefulness and effectiveness of the proposed metasurface.

For this paper, the proposed metasurface unit cell was designed at 297.2 MHz for 7-T MRI. Indeed, field enhancement is more needed in a low-field MRI system since the SNR in such a system is low. However, a decrease in B_0 leads to an increase in the wavelength, and thus an increase in the physical size of a unit cell of metasurface. It imposes challenges on reducing the cell size. With the intrinsic compactness, a space-filling curve like the Hilbert curve with further design, optimization, and modifications can be a promising solution.

VI. CONCLUSION

A subwavelength metasurface resonator based on a Hilbert curve is presented for field enhancement deep into the imaging volume for an RF coil for 7-T MRI. A unit cell of a TEM coil was used in the study. The coil and a fourth-order Hilbert curve-based unit cell were fabricated for experiments. The effectiveness of RF field enhancement was successfully demonstrated using both simulation and experimental data.

A magnetic field enhancement of more than four times at the depth of 13.5 cm into the imaging volume is observed experimentally. A circuit model is proposed for a fast estimation of the resonance of Hilbert curve of a given order

with significantly improved accuracy. Due to the nature of the Hilbert curve geometry, the proposed metasurface resonator is compact at a working frequency of 297.2 MHz. It is lightweight and can be manufactured using a standard PCB technology on rigid or flexible substrates. The possibility of being integrated to an existing MRI coil is shown and discussed.

It is an initial demonstration of a proof of concept for the application of a metasurface of this kind for field enhancement. The proposed design provides a solution that can be used to improve the performance of a receive RF coil. Issues such as the compatibility of the proposed metasurface to different MRI coils and to an MRI system need to be addressed in detail in the near future. The design can potentially be extended to an MRI system of other field strengths (1.5 and 3 T).

REFERENCES

- [1] P. C. Lauterbur, "Image formation by induced local interactions: Examples employing nuclear magnetic resonance," *Nature*, vol. 242, pp. 190–191, Mar. 1973.
- [2] J. T. Vaughan and J. R. Griffiths, *RF Coils for MRI*. Hoboken, NJ, USA: Wiley, 2012.
- [3] T. J. Cui, D. R. Smith, and R. P. Liu, *Metamaterials*. New York, NY, USA: Springer, 2010.
- [4] N. I. Zheludev and Y. S. Kivshar, "From metamaterials to metadevices," *Nature Mater.*, vol. 11, no. 11, pp. 917–924, 2012.
- [5] C. L. Holloway, E. F. Kuester, J. A. Gordon, J. O'Hara, J. Booth, and D. R. Smith, "An overview of the theory and applications of metasurfaces: The two-dimensional equivalents of metamaterials," *IEEE Antennas Propag. Mag.*, vol. 54, no. 2, pp. 10–35, Apr. 2012.
- [6] S. B. Glybovski, S. A. Tretyakov, P. A. Belov, Y. S. Kivshar, and C. R. Simovski, "Metasurfaces: From microwaves to visible," *Phys. Rep.*, vol. 634, pp. 1–72, May 2016.
- [7] D. R. Smith, W. J. Padilla, D. C. Vier, S. C. Nemat-Nasser, and S. Schultz, "Composite medium with simultaneously negative permeability and permittivity," *Phys. Rev. Lett.*, vol. 84, no. 18, p. 4184, 2000.
- [8] J. B. Pendry, "Negative refraction makes a perfect lens," *Phys. Rev. Lett.*, vol. 85, no. 18, p. 3966, 2000.
- [9] J. B. Pendry, D. Schurig, and D. R. Smith, "Controlling electromagnetic fields," *Science*, vol. 312, no. 5781, pp. 1780–1782, 2006.
- [10] M. C. K. Wiltshire, J. B. Pendry, I. R. Young, D. J. Larkman, D. J. Gilderdale, and J. V. Hajnal, "Microstructured magnetic materials for RF flux guides in magnetic resonance imaging," *Science*, vol. 291, no. 5505, pp. 849–851, 2001.
- [11] M. J. Freire, R. Marques, and L. Jelinek, "Experimental demonstration of a $\mu = -1$ metamaterial lens for magnetic resonance imaging," *Appl. Phys. Lett.*, vol. 93, no. 23, p. 231108, 2008.
- [12] X. Radu, X. Dardenne, and C. Craeye, "Experimental results and discussion of imaging with a wire medium for MRI imaging applications," in *Proc. IEEE Antennas Propag. Soc. Int. Symp.*, Jun. 2007, pp. 5499–5502.
- [13] X. Radu, D. Garray, and C. Craeye, "Toward a wire medium endoscope for MRI imaging," *Metamaterials*, vol. 3, no. 2, pp. 90–99, 2009.
- [14] A. P. Slobozhanyuk *et al.*, "Enhancement of magnetic resonance imaging with metasurfaces," *Adv. Mater.*, vol. 28, no. 9, pp. 1832–1838, 2016.
- [15] A. Shchelokova *et al.*, "Wireless coil based on meta-technologies for MRI implementations," in *Proc. ISMRM*, Apr. 2017.
- [16] R. Schmidt, A. Slobozhanyuk, P. Belov, and A. Webb, "Flexible and compact hybrid metasurfaces for enhanced ultra high field *in vivo* magnetic resonance imaging," *Sci. Rep.*, vol. 7, no. 1, p. 1678, 2017.
- [17] K. J. Vinoy, K. A. Jose, V. K. Varadan, and V. V. Varadan, "Hilbert curve fractal antenna: A small resonant antenna for VHF/UHF applications," *Microw. Opt. Technol. Lett.*, vol. 29, no. 4, pp. 215–219, 2001.
- [18] J. McVay, N. Engheta, and A. Hoorfar, "High impedance metamaterial surfaces using Hilbert-curve inclusions," *IEEE Microw. Wireless Compon. Lett.*, vol. 14, no. 3, pp. 130–132, Mar. 2004.
- [19] J. Chen, Z.-B. Weng, Y.-C. Jiao, and F.-S. Zhang, "Lowpass filter design of Hilbert curve ring defected ground structure," *Prog. Electromagn. Res.*, vol. 70, no. 70, pp. 269–280, 2007.
- [20] J. McVay, A. Hoorfar, and N. Engheta, "Space-filling curve RFID tags," in *Proc. IEEE Radio Wireless Symp.*, Oct. 2006, pp. 199–202.
- [21] H. Sagan, *Space-Filling Curves*. New York, NY, USA: Springer, 2012.
- [22] K. J. Vinoy, K. A. Jose, V. K. Varadan, and V. V. Varadan, "Resonant frequency of Hilbert curve fractal antennas," in *Proc. IEEE Antennas Propag. Soc. Int. Symp.*, Boston, MA, USA, vol. 3, Jul. 2001, pp. 648–651.
- [23] E. B. Rosa, "The self and mutual inductances of linear conductors," *Bull. Bur. Standards*, vol. 4, no. 2, pp. 301–344, 1908, doi: 10.6028/bulletin.088.
- [24] J. D. Jackson, *Classical Electrodynamics*, 3rd ed. New York, NY, USA: Wiley, 1999.
- [25] M. J. Freire, L. Jelinek, R. Marques, and M. Lapine, "On the applications of $\mu_r = -1$ metamaterial lenses for magnetic resonance imaging," *J. Magn. Reson.*, vol. 203, no. 1, pp. 81–90, 2010.
- [26] X. Chen, T. M. Grzegorzczak, B.-I. Wu, J. Pacheco, Jr., and J. A. Kong, "Robust method to retrieve the constitutive effective parameters of metamaterials," *Phys. Rev. E, Stat. Phys. Plasmas Fluids Relat. Interdiscip. Top.*, vol. 70, no. 1, p. 016608, 2004.
- [27] J. T. Vaughan, H. P. Hetherington, J. O. Otu, J. W. Pan, and G. M. Pohost, "High frequency volume coils for clinical NMR imaging and spectroscopy," *Magn. Reson. Med.*, vol. 32, no. 2, pp. 206–218, 1994.
- [28] A. J. E. Raaijmakers, P. R. Luijten, and C. A. T. van den Berg, "Dipole antennas for ultrahigh-field body imaging: A comparison with loop coils," *NMR Biomed.*, vol. 29, no. 9, pp. 1122–1130, 2016.
- [29] Y. Gao and I. Wolff, "Miniature electric near-field probes for measuring 3-D fields in planar microwave circuits," *IEEE Trans. Microw. Theory Techn.*, vol. 46, no. 7, pp. 907–913, Jul. 1998.
- [30] J. Shi, M. A. Cracraft, K. P. Slattery, M. Yamaguchi, and R. E. DuBroff, "Calibration and compensation of near-field scan measurements," *IEEE Trans. Electromagn. Compat.*, vol. 47, no. 3, pp. 642–650, Aug. 2005.
- [31] E. Motovilova and S. Y. Huang, "A Hilbert curve based metasurface for B_1^+ -field enhancement," in *Proc. ISMRM*, Jun. 2018.
- [32] S. R. Best and J. D. Morrow, "The effectiveness of space-filling fractal geometry in lowering resonant frequency," *IEEE Antennas Wireless Propag. Lett.*, vol. 1, pp. 112–115.